Generalized Likelihood Ratio Tests for Linear Structure Detection in SAR Images

Nicolas Gasnier, Loïc Denis, Florence Tupin

Generalized Likelihood Ratio Tests for Linear Structure Detection in SAR Images

Nicolas Gasnier[a], Loïc Denis[b], and Florence Tupin[a]
[a]LTCI, Télécom Paris, Institut Polytechnique de Paris, 91120 Palaiseau, France
[b]Univ Lyon, UJM-Saint-Étienne, CNRS, Institut d'Optique Graduate School, Laboratoire Hubert Curien UMR 5516, F-42023, Saint-Etienne, France

Abstract

The detection of linear structures in Synthetic Aperture Radar images is often used as a first step for further processing such as the extraction of road and river networks. In this paper, we propose a new method based on the Generalized Likelihood Ratio Test (GLRT) framework to evaluate at each pixel the likelihood of the presence of a linear structure. Results are presented on Sentinel-1 images and compared with a state-of-the-art method, also derived from the GLRT framework but with a simpler model of the lines. In our experiments, our method produces far fewer false positives than the reference method.

1 Introduction

With the increasing availability of Synthetic Aperture Radar (SAR) images, a lot of applications have been developed to extract useful information from these data for various fields (urban areas monitoring, environmental surveillance,...). For some of these applications such as river or road network extraction, the detection of linear structures is a crucial step of the processing.

Linear structures can be characterized as a set of contiguous pixels in a long and thin layout (width of a few pixels) whose reflectivity is significantly different from the reflectivity of the background. Linear structures, that are not necessarily straight-lined, can be dark (rivers and roads for most sensors such as Sentinel 1, TerraSAR-X,...) or bright (rivers for near-nadir sensors like KaRIn sensor in the future SWOT mission [3] or long, linear man-made structures).
Their detection is particularly difficult in SAR images because of the high level of speckle noise: the detected intensity can be very different from the underlying reflectivity. Because of these fluctuations, the methods that have been developed for optical images [4, 2, 1, 10, 7] cannot be directly applied to SAR images. To cope with the speckle, a first denoising step can be applied to reduce the noise level, but that approach comes at the cost of additional computational time, the loss of some details or the appearance of denoising artifacts that may respectively lead to false negatives or false positives in the subsequent linear structure detection.
In the past 30 years, several methods have been proposed to address the problem of linear structure detection in noisy SAR images: Hellwich *et al.* [5] combine intensity and coherence information, Tupin *et al.* [8] combine the results of a ratio-based line detector and a cross-correlation-based line detector and can still be considered as a reference method today.

In this paper, we propose a new approach based on a local translation invariance property of linear structures to derive a hypothesis test and decide in favor of the presence or the absence of a line. This leads to a detection map. This map can subsequently be used for other processing steps, for example to retrieve the network through linear programming [6].

2 Overview of the method

In this section, we introduce the model that grounds our method and describe how our criterion is defined. Most often, only one type of linear structure is sought: either bright lines over a darker background or dark lines in a brighter area (e.g., roads or rivers). A feature of our approach is to clearly distinguish those two cases. In the following, we consider the task of detecting dark linear structures. The adaptation to bright structures is straightforward.

2.1 GLRT criterion for linear structure detection

Our detection criterion evaluates the likelihood of the presence of a linear structure centered at a given pixel k by comparing two hypotheses:

- H_0 : there is no linear structure
- H_1: there is a linear structure

The comparison between these two hypotheses is done by determining which hypothesis best explains the observed patch $\boldsymbol{I}_k \in \mathbb{R}^{(2N+1)\times(2N+1)}$ (i.e., the vector formed by

the concatenation of all the intensities inside a small square window centered at the k-th pixel). In this paper, we assume that the null hypothesis H_0 ("no linear structure") corresponds to a patch with a constant reflectivity[1] R. Under the alternative hypothesis H_1, a linear structure is present and the reflectivities inside the patch are shift-invariant in the direction of the structure, see **Figure 2**.

The likelihood of each hypothesis depends on several unknown parameters: the constant reflectivity R, under H_0; the reflectivity profile $\boldsymbol{P}$ and the line direction θ, under H_1. These unknown parameters can be obtained by the maximum likelihood estimator. The decision in favor of hypothesis H_0 or H_1 can be made based on the generalized likelihood ratio, i.e., the ratio of the likelihoods of each hypothesis where unknown parameters are replaced by their maximum likelihood estimates[9]:

$$\text{GLRT}_k = \frac{\text{p}(\boldsymbol{I}_k|H_1, \widehat{\boldsymbol{P}}, \widehat{\theta})}{\text{p}(\boldsymbol{I}_k|H_0, \widehat{R})}\,. \tag{1}$$

This GLRT must be repeated at each pixel k of the image. Computing the maximum likelihood estimators is simplified when log-transformed intensities are considered. Under Goodman's fully-developed speckle model, the log-transformed intensities follow a Fisher-Tippett distribution:

$$\text{p}(y|x) = \frac{L^L}{\Gamma(L)} e^{L(y-x)} \exp(-Le^{y-x})\,, \tag{2}$$

where y is the log of the intensity at a given pixel, x is the log of the reflectivity at that pixel and L is the number of looks of the image. In order to obtain closed-form expressions for the likelihood estimators and GLRTs that can be efficiently performed, we approximate this distribution by a Gaussian distribution:

$$\text{p}(y|\mu) \simeq f(x) = \frac{1}{\sigma\sqrt{2\pi}}\, \text{e}^{-\frac{1}{2}\left(\frac{y-\mu}{\sigma}\right)^2}, \tag{3}$$

where $\sigma = \sqrt{\psi(1, L)}$, and $\mu = x - \log(L) + \psi(L)$ with ψ being respectively the polygamma and the digamma function to match the standard deviation and the expected value of the previous distribution. This approximation is reasonably precise for multi-look SAR images. **Figure 1** compares the distribution of the log-transformed speckle for $L = 4.4$ corresponding to Sentinel-1 full-resolution GRD images acquired in IW mode. The two distributions are close. While the differences may impact the quality of estimators of the reflectivity, for hypothesis testing purposes the impact is negligible at $L = 4.4$.

Under these assumptions, the biased log-reflectivity $r = \log(R) - \log(L) + \psi(L)$ of the homogeneous background under H_0 hypothesis can be estimated from the mean of the log-transformed intensities y of the patch. The estimation of the reflectivity profile and of the line orientation is described in more details in the next section.

[1]This assumption may seem too restrictive. Inhomogeneous reflectivity distributions inside the patch that can neither be modeled by a constant nor by a shift-invariant profile lead to similar likelihood values under H_0 and H_1, they therefore do not lead to false detections. The simplifying assumption of a constant reflectivity under H_0 therefore does not limit the applicability of the method to homogeneous or linear structures.

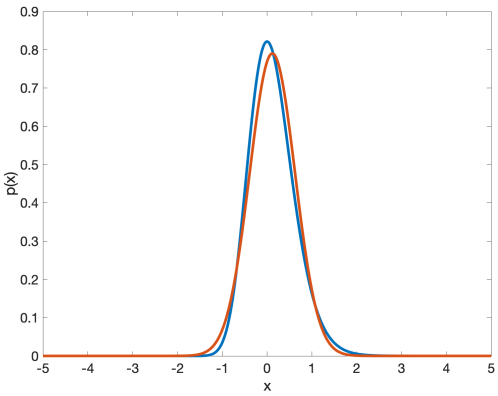

Figure 1 Fisher-Tippett distribution (orange) and its Gaussian approximation (blue) for L=4.4.

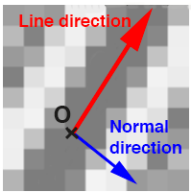

Figure 2 The profile of the reflectivity of the linear structure is defined in the direction that is normal to the direction of the linear structure

When the estimates of the (biased) log-reflectivities of the k-th patch $\hat{r}_k\mathbf{1}$, under H_0, and $\widehat{\boldsymbol{r}}_{k,\hat{\theta}}$, under H_1, are substituted in the definition of GLRT_k in equation (1), we obtain, under our Gaussian approximation:

$$\log(\text{GLRT}_k) = \frac{1}{2}||\boldsymbol{y}_k - \hat{r}_k\mathbf{1}||^2 - \frac{1}{2}||\boldsymbol{y}_k - \widehat{\boldsymbol{r}}_{k,\hat{\theta}}||^2\,, \tag{4}$$

where $\mathbf{1}$ is a vector of ones with the same dimension as $\boldsymbol{y}_k$ (the number of pixels in a patch).

2.2 Modeling of a linear structure

Before describing the linear structure parameters, we first define how a linear structure can be characterized at the scale of a patch. Considering a patch of size $(2N + 1) \times (2N + 1)$, centered at the k-th pixel, with a dark line that crosses the patch as depicted in **Figure 2**, two ingredients define our model: (i) the reflectivity is lower in the central line than farther from the line, and (ii) the reflectivity distribution is invariant in the direction of the line. Throughout the paper, the 1D distribution of the reflectivity along the direction orthogonal to the line is called the *reflectivity profile*.

Beyond the shift-invariance of the reflectivity in the direction of the line, we also require the profile to be symmetrical with respect to the median axis of the line. This is useful to improve the localization of the linear structure and to reduce the number of false positives.

2.3 Estimation of the local orientation of the linear structure

The maximum likelihood estimate $\widehat{\theta}$ of the angle of the linear structure in the patch is obtained by uniformly sampling the orientations (60 steps are used in the range $[0, \pi]$ in our experiments). The largest value of GLRT_k is retained among all values computed for the set of orientations considered.

2.4 Estimation of the reflectivity profile of the linear structure

The first step to estimate the reflectivity profile of the linear structure is to model the mapping from a 1D profile $\boldsymbol{p}_{k,\theta}$ to a 2D patch $\boldsymbol{r}_{k,\theta}$. In order to cover a patch of size $(2N+1) \times (2N+1)$ pixels for all orientations of the line, the 1D profile has to cover $\sqrt{2}(2N+1)$ pixels. Since we consider profiles that are symmetrical with respect to the central line, defining the profile only for the first $\sqrt{2}(N+1)$ pixels from the patch center O is sufficient. The mapping operation amounts to interpolating the 1D profile at each pixel of the 2D patch according to the distance of the pixel to the line that goes through O and that forms an angle θ with respect to the horizontal direction. This interpolation operation is a linear transform characterized by a matrix $\boldsymbol{M}_\theta$ of size $(2N+1) \cdot (2N+1) \times \sqrt{2}(N+1)$:

$$\boldsymbol{r}_{k,\theta} = \boldsymbol{M}_\theta \, \boldsymbol{p}_{k,\theta} \tag{5}$$

The second step is to compute the maximum likelihood estimate $\widehat{\boldsymbol{p}}_\theta$ of the reflectivity profile of a linear structure oriented in the direction θ. Under our Gaussian approximation, this corresponds to the least squares solution:

$$\widehat{\boldsymbol{p}}_{k,\theta} = \boldsymbol{M}_\theta^{\text{pinv}} \boldsymbol{y}_k \tag{6}$$

where $\boldsymbol{M}_\theta^{\text{pinv}}$ is the Moore-Penrose pseudoinverse of $\boldsymbol{M}_\theta$.

In order to force the reflectivity at the center of the line structure to be the minimum of the reflectivity profile, a thresholding operation is added after estimating the maximum likelihood profile:

$$\widehat{\boldsymbol{p}}^+_{k,\theta} = \max\left\{\widehat{\boldsymbol{p}}_{k,\theta}, [\widehat{\boldsymbol{p}}_{k,\theta}]_1\right\} , \tag{7}$$

where the maximum is applied component-wise and $[\widehat{\boldsymbol{p}}_\theta]_1$ is the value of the log-reflectivity at the center of the profile (first element of the vector). In the thresholded profile $\widehat{\boldsymbol{p}}^+_\theta$, no reflectivity can be lower than the reflectivity at the center of the profile. If, rather than dark lines, bright lines were to be detected, this maximum should be replaced by a minimum to define a profile $\widehat{\boldsymbol{p}}^-_\theta$ where no reflectivity is ever brighter than the reflectivity at the center of the line.
From this estimated profile, the estimated reflectivities inside the patch centered on pixel k are obtained by applying the interpolation operator $\boldsymbol{M}_\theta$:

$$\widehat{\boldsymbol{r}}_{k,\theta} = \boldsymbol{M}_\theta \, \widehat{\boldsymbol{p}}^+_{k,\theta} \, . \tag{8}$$

The maximum likelihood orientation of the line structure in the k-th patch is obtained by:

$$\widehat{\theta} = \arg\max_\theta \; \|\boldsymbol{y}_k - \boldsymbol{M}_\theta \, \widehat{\boldsymbol{p}}^+_{k,\theta}\|^2 \, . \tag{9}$$

The computation of $\text{GLRT}_{k,\theta}$ is then obtained by the application of equation (**??**) for a given orientation θ. The detection criterion at pixel k and orientation θ can be expanded as follows:

$$\begin{aligned} \log \text{GLRT}_{k,\theta} &= \tfrac{1}{2}||\boldsymbol{y}_k - \hat{r}_k \mathbf{1}||^2 - \tfrac{1}{2}||\boldsymbol{y}_k - \widehat{\boldsymbol{r}}_{k,\theta}||^2 \\ &= \tfrac{1}{2}||\hat{r}_k \mathbf{1}||^2 - \boldsymbol{y}_k^{\mathrm{T}} \hat{r}_k \mathbf{1} + \boldsymbol{y}_k^{\mathrm{T}} \widehat{\boldsymbol{r}}_{k,\theta} - \tfrac{1}{2}||\widehat{\boldsymbol{r}}_{k,\theta}||^2 \end{aligned} \tag{10}$$

where the maximum likelihood estimate of the reflectivity $\hat{r}_k$ of a constant patch is the mean log intensity in the patch: $\hat{r}_k = \mathbf{1}^{\mathrm{T}} \boldsymbol{y}_k / \mathbf{1}^{\mathrm{T}} \mathbf{1} = \frac{1}{(2N+1)^2} \sum_i [\boldsymbol{y}_k]_i$.

A straightforward implementation of (10) requires computing, at each pixel of the $H \times W$ pixels SAR image, norms or scalar products of $\hat{r}_k$ and $\widehat{\boldsymbol{r}}_{k,\theta}$. The estimate $\hat{r}_k$ is obtained in $(2N+1)^2 = \mathcal{O}[N^2]$ multiplications. The estimate $\widehat{\boldsymbol{r}}_{k,\theta}$ requires $2(2N+1)^2\sqrt{2}(N+1) = \mathcal{O}[N^3]$ multiplications. The total cost for evaluating $\log \text{GLRT}_{k,\theta}$ at all pixels and for T angles θ is thus $\mathcal{O}[WHTN^3]$. We show that the algorithmic complexity can be reduced to $\mathcal{O}[WHTN^2 \log(WH)]$ (and even to $\mathcal{O}[WHTN \log(WH)]$ if the constraint (7) is dropped) with discrete correlations computed in Fourier domain using fast Fourier transforms.
Note that any product of the form $\boldsymbol{w}^{\mathrm{T}} \boldsymbol{y}_k$ corresponds to a 2D discrete correlation of the log-transformed image $\boldsymbol{y}$ with the 2D filter whose 1D representation in lexicographic order is $\boldsymbol{w}$: $\boldsymbol{w}^{\mathrm{T}} \boldsymbol{y}_k = [\text{correl}(\boldsymbol{y}, \boldsymbol{w})]_k$. This correlation can be computed efficiently using 2D fast Fourier transforms: $\text{correl}(\boldsymbol{y}, \boldsymbol{w}) = \texttt{FFT}_{\text{2D}}^{-1}\left[\texttt{FFT}_{\text{2D}}(\boldsymbol{y}) \cdot \text{conj}\left(\texttt{FFT}_{\text{2D}}(\boldsymbol{w})\right)\right]$ where the conjugate operation conj() and the product $\cdot$ are performed element-wise.
The first term $\frac{1}{2}||\hat{r}_k \mathbf{1}||^2$ in equation (10) corresponds to $\frac{1}{2(2N+1)^2}[\text{correl}(\boldsymbol{y}, \mathbf{1})]_k^2$, the second term $-\boldsymbol{y}_k^{\mathrm{T}} \hat{r}_k \mathbf{1}$ to $-\frac{1}{(2N+1)^2}[\text{correl}(\boldsymbol{y}, \mathbf{1})]_k^2$, their sum is thus equal to $-\frac{1}{2(2N+1)^2}[\text{correl}(\boldsymbol{y}, \mathbf{1})]_k^2$, which can be computed in $\mathcal{O}[WH \log(WH)]$ operations with fast Fourier transforms.
The third and fourth terms require the estimation of $\widehat{\boldsymbol{r}}_{k,\theta}$ using equations (6), (7) and (8). The i-th element of $\widehat{\boldsymbol{p}}_{k,\theta}$ corresponds to the product of the i-th row of matrix $\boldsymbol{M}_\theta^{\text{pinv}}$ and the log-transformed data $\boldsymbol{y}_k$, which can be expressed using a discrete correlation: $[\widehat{\boldsymbol{p}}_{k,\theta}]_i = [\text{correl}(\boldsymbol{y}, [\boldsymbol{M}_\theta^{\text{pinv}}]_{i,\bullet})]_k$, where the notation $[\boldsymbol{M}_\theta^{\text{pinv}}]_{i,\bullet}$ indicates the i-th row of matrix $\boldsymbol{M}_\theta^{\text{pinv}}$. All profiles $\widehat{\boldsymbol{p}}^+_{k,\theta}$ can thus be computed in $\mathcal{O}[WHTN \log(WH)]$ operations. Rather than computing $\widehat{\boldsymbol{r}}_{k,\theta}$ for all θ and k before deriving $\boldsymbol{y}_k^{\mathrm{T}} \widehat{\boldsymbol{r}}_{k,\theta}$, it is more efficient to compute $(\boldsymbol{M}_\theta^{\mathrm{T}} \boldsymbol{y}_k)^{\mathrm{T}} \widehat{\boldsymbol{p}}^+_{k,\theta}$ since $[\boldsymbol{M}_\theta^{\mathrm{T}} \boldsymbol{y}_k]_i = [\text{correl}(\boldsymbol{y}, [\boldsymbol{M}_\theta]_{\bullet,i})]_k$. The third term is thus obtained in an additional $\mathcal{O}[WHTN \log(WH)]$ operations. The computation of the fourth term is the most costly. To reduce the cost, we use the singular value decomposition (SVD) of matrix $\boldsymbol{M}_\theta$: $\boldsymbol{M}_\theta = \boldsymbol{U}_\theta \boldsymbol{S}_\theta \boldsymbol{V}_\theta^{\mathrm{T}}$ where $\boldsymbol{U}_\theta$ is a $(2N+1)^2 \times (2N+1)^2$ unitary matrix, $\boldsymbol{V}_\theta$ is a $\sqrt{2}(N+1) \times \sqrt{2}(N+1)$ unitary matrix, and $\boldsymbol{S}_\theta$ is rectangular with zeros outside the main diagonal. The expansion $\|\boldsymbol{M}_\theta \widehat{\boldsymbol{p}}^+_{k,\theta}\|^2 = \widehat{\boldsymbol{p}}^{+\mathrm{T}}_{k,\theta} \boldsymbol{M}_\theta^{\mathrm{T}} \boldsymbol{M}_\theta \widehat{\boldsymbol{p}}^+_{k,\theta} = \widehat{\boldsymbol{p}}^{+\mathrm{T}}_{k,\theta} \boldsymbol{V}_\theta \boldsymbol{S}_\theta^2 \boldsymbol{V}_\theta^{\mathrm{T}} \widehat{\boldsymbol{p}}^+_{k,\theta}$

shows that

$$\|\widehat{\boldsymbol{r}}_{k,\theta}\|^2 = \sum_{i=1}^{\sqrt{2}(N+1)} [\boldsymbol{S}_\theta]_{i,i}^2 ([\boldsymbol{V}_\theta]_{\bullet,i}^{\mathrm{T}} \widehat{\boldsymbol{p}}_{k,\theta}^{+})^2 \qquad (11)$$

which can be computed for all k and all θ in $\mathcal{O}[WHTN^2]$ operations once $\widehat{\boldsymbol{p}}_{k,\theta}^{+}$ has been computed. In the absence of the non-linear thresholding operation (7), it would be possible to compute $\|\widehat{\boldsymbol{r}}_{k,\theta}\|^2$ by discrete correlations between the SAR image $\boldsymbol{y}$ and the columns of the SVD of matrix $\boldsymbol{M}_\theta \boldsymbol{M}_\theta^{\text{pinv}}$ in $\mathcal{O}[WHTN\log(WH)]$ operations.
The complete algorithm has a complexity $\mathcal{O}[WHTN(N + \log(HW))]$ to compute the detection map. It is summarized below:

Algorithm to compute a line detection map

Input: $\boldsymbol{y}$ ($H \times W$ pixels SAR image)
Output: **log GLRT** ($H \times W$ pixels detection map)

{compute first two terms}
$\boldsymbol{c} \leftarrow \text{correl}(\boldsymbol{y}, \mathbf{1})$
for $k = 1$ to HW **do**
  $[\textbf{log GLRT}]_k \leftarrow -\frac{1}{2(2N+1)^2}[\boldsymbol{c}]_k^2$
end for
{compute last two terms}
$\boldsymbol{d}_{\max} \leftarrow \mathbf{0}$ ($H \times W$ temporary map)
for $\theta = \theta_1$ to θ_T **do**
  $\boldsymbol{d} \leftarrow \mathbf{0}$ ($H \times W$ temporary map)
  $\{\boldsymbol{U}_\theta, \boldsymbol{S}_\theta, \boldsymbol{V}_\theta\} \leftarrow \texttt{SVD}(\boldsymbol{M}_\theta)$
  for $i = 1$ to $\sqrt{2}(N+1)$ **do**
    $[\boldsymbol{p}]_{\bullet,i} \leftarrow \text{correl}(\boldsymbol{y}, [\boldsymbol{M}_\theta^{\text{pinv}}]_{i,\bullet})$
    $[\boldsymbol{p}]_{\bullet,i} \leftarrow \max\big([\boldsymbol{p}]_{\bullet,i}, [\boldsymbol{p}]_{\bullet,1}\big)$
    $\boldsymbol{d} \leftarrow \boldsymbol{d} + \text{correl}(\boldsymbol{y}, [\boldsymbol{M}_\theta]_{\bullet,i}) \cdot [\boldsymbol{p}]_{\bullet,i}$ (3rd term)
    $\boldsymbol{t} \leftarrow \mathbf{0}$ (HW temporary array)
    for $j = 1$ to $\sqrt{2}(N+1)$ **do**
      $\boldsymbol{t} \leftarrow \boldsymbol{t} + [\boldsymbol{V}_\theta]_{j,i}[\widehat{\boldsymbol{p}}]_{\bullet,j}$
    end for
    $\boldsymbol{d} \leftarrow \boldsymbol{d} - \frac{1}{2}[\boldsymbol{S}_\theta]_{i,i}^2 \boldsymbol{t}^2$ (4th term)
  end for
  $\boldsymbol{d}_{\max} \leftarrow \max(\boldsymbol{d}_{\max}, \boldsymbol{d})$
end for
log GLRT $\leftarrow$ **log GLRT** $+ \boldsymbol{d}_{\max}$

3 Potential adaptations of the method

Some of the possible adaptations of the method are discussed in this section.

3.1 Multiscale processing

As the maximum width of the structures that can be detected are limited by the size of the patch, the detection of large structures can be computationally difficult. To cope with this, a multiscale processing approach can be used by applying the detector on rescaled images. Combinations of multiple scales can be done by adding the rescaled responses of the detector.

3.2 Constraint over the symmetry of the profile

Assuming that the background is homogeneous, the rate of false detection can be decreased by enforcing the symmetry of the profile. This modification changes the shape of the vector P representing the profile as storing the half profile is now sufficient and changes the matrix M_θ and M_θ^+.
This constraint has been applied in the tests presented in the next section.

3.3 Adaptation to river detection in near-nadir sensors

On near-nadir sensors like KaRIn in the future SWOT mission, flat surfaces like rivers are seen as bright linear structures on a dark background. The proposed detector can easily be adapted to this configuration by modifying the constraint presented in section 2.4: instead of preventing the profile from being darker than its center as for dark lines detections, the constraint prevents the profile from being brighter.

4 Results

This section presents the results of the proposed line detector applied to various Sentinel 1 SAR images. The results are compared to the response of the linear structures detector presented in [8]. The results presented here have been obtained using our line detector [2] with a symmetry constraint on three scales (with rescaling factors of 3,2 and 1) and summing the results.

All images are Sentinel 1 Full-resolution GRD images acquired in IW mode with dark linear structures corresponding to rivers. **Figure 3** shows a comparison of the two detectors on linear structures corresponding to the Esk River near Carwinley (United Kindom). On **Figure 4** the linear structures correspond to the Vilaine and Oust rivers near Redon (France).On **Figure 7** the linear structures correspond to the Loire river in Angers (France) and to smaller rivers nearby.

Figure 5 shows one example over the city of Des Moines (Iowa, USA) with the Racoon River. A ground truth (d) for the "line" class (red line) and for the "no line" class (green rectangle) has been used to draw the receiver operating curves (ROC) for both detectors presented **Figure 6**. On the ROC curves, the proposed detector is better than the state-of-the-art detector, as for any given false positive rate, its true positive rate is higher.
The proposed algorithm response clearly has fewer false positive while maintaining a good detection of the linear structures. More importantly, the artifacts created by the proposed method are not line-shaped unlike those of the reference method and will be less troublesome for some

[2] The code of the line detector is available at https://gitlab.telecom-paris.fr/ring/glrt_based_lines_detector

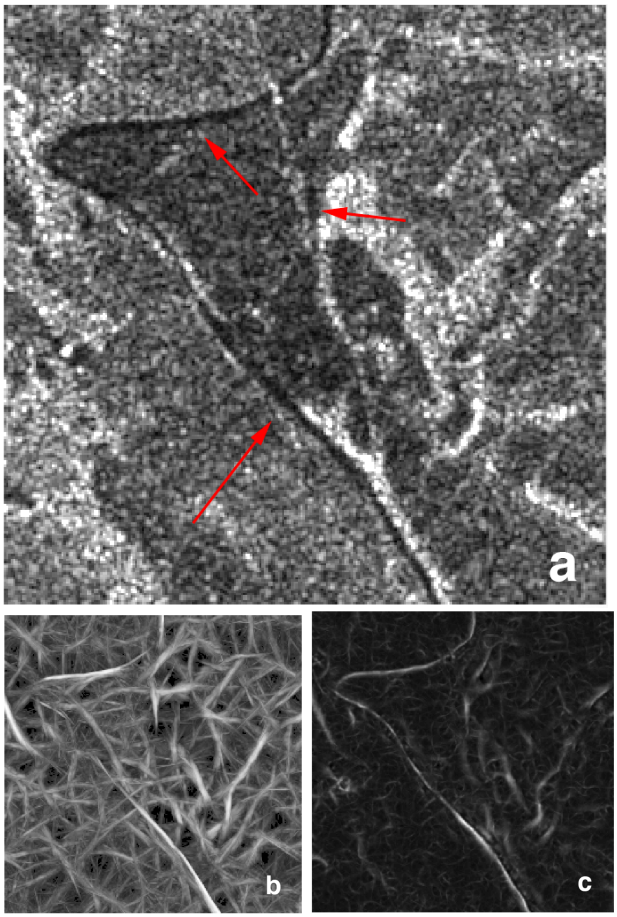

Figure 3 Comparison between the proposed detector (c) and the state-of-the-art detector (b) for one GRD image with linear structures highlighted by red arrows (a)

further processing such as shortest path finding.

5 Conclusion

This paper proposes a new approach to detect linear structures in a SAR image which can have multiple applications such as road-network or river extraction. In our comparisons on Sentinel 1 image, the proposed method shows an improved detection performance compared to a reference line detection method.

6 Acknowledgements

The authors would like to thank the Centre National d'Études Spatiales and C-S GROUP for their fundings.

7 Literature

[1] F. Deschênes and D. Ziou. Detection of line junctions and line terminations using curvilinear features. *Pattern Recognition Letters*, 21(6):637 – 649, 2000.

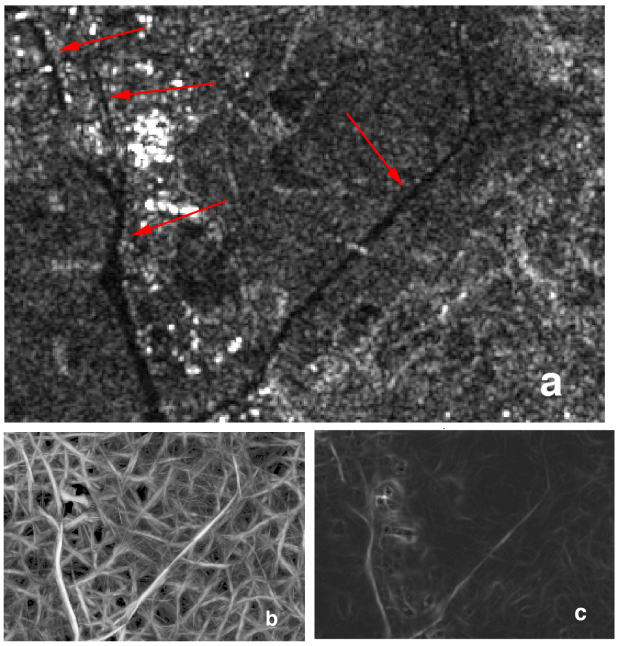

Figure 4 Comparison between the proposed detector (c) and the state-of-the-art detector (b) for one GRD image with linear structures highlighted by red arrows (a)

[2] Martin A Fischler, Jay M Tenenbaum, and Hans Christoph Wolf. Detection of roads and linear structures in low-resolution aerial imagery using a multisource knowledge integration technique. In *Readings in Computer Vision*, pages 741–752. Elsevier, 1987.

[3] R. Fjørtoft, J. Gaudin, N. Pourthié, J. Lalaurie, A. Mallet, J. Nouvel, J. Martinot-Lagarde, H. Oriot, P. Borderies, C. Ruiz, and S. Daniel. Karin on swot: Characteristics of near-nadir ka-band interferometric sar imagery. *IEEE Transactions on Geoscience and Remote Sensing*, 52(4):2172–2185, April 2014.

[4] D. Geman and B. Jedynak. An active testing model for tracking roads in satellite images. *IEEE Transactions on Pattern Analysis and Machine Intelligence*, 18(1):1–14, Jan 1996.

[5] Olaf Hellwich, Ivan Laptev, and Helmut Mayer. Extraction of linear objects from interferometric sar data. *International Journal of Remote Sensing*, 23(3):461–475, 2002.

[6] N. Merlet and J. Zerubia. New prospects in line detection by dynamic programming. *IEEE Transactions on Pattern Analysis and Machine Intelligence*, 18(4):426–431, April 1996.

[7] S. Movaghati, A. Moghaddamjoo, and A. Tavakoli. Road extraction from satellite images using particle filtering and extended kalman filtering. *IEEE Transactions on Geoscience and Remote Sensing*, 48(7):2807–2817, July 2010.

[8] F. Tupin, H. Maitre, J. . Mangin, J. . Nicolas, and E. Pechersky. Detection of linear features in sar images: application to road network extraction. *IEEE Transactions on Geoscience and Remote Sensing*, 36(2):434–453, March 1998.

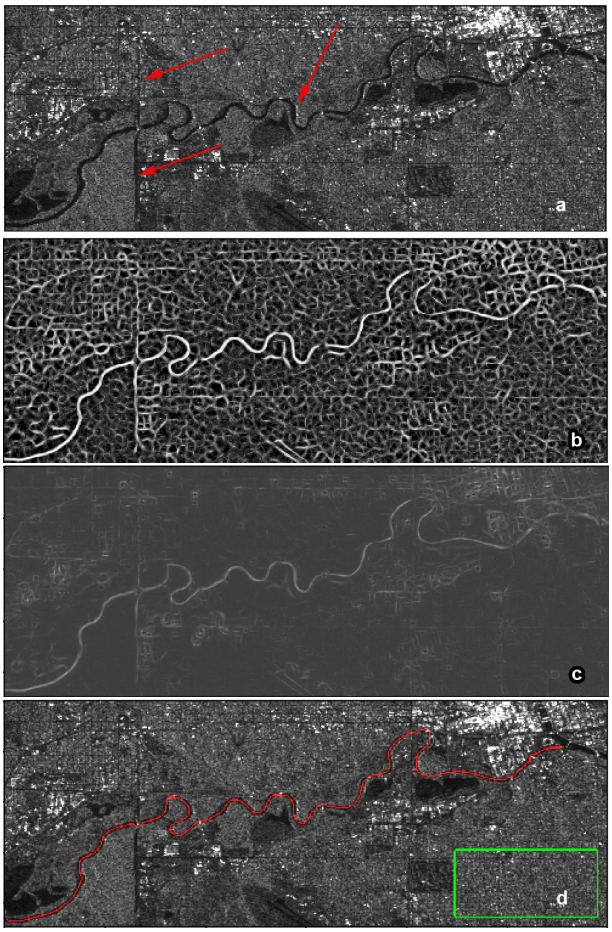

Figure 5 Comparison between the proposed detector (c) and the state-of-the-art detector (b) for one GRD image with linear structures highlighted by red arrows (a). (d) shows the "line" area (red line) and the "no line" area (green rectangle) used to compute the ROC curve.

[9] Harry L Van Trees. *Detection, estimation, and modulation theory, part I: detection, estimation, and linear modulation theory*. John Wiley & Sons, 2004.

[10] G. J. Vanderbrug. Line detection in satellite imagery. *IEEE Transactions on Geoscience Electronics*, 14(1):37–44, Jan 1976.

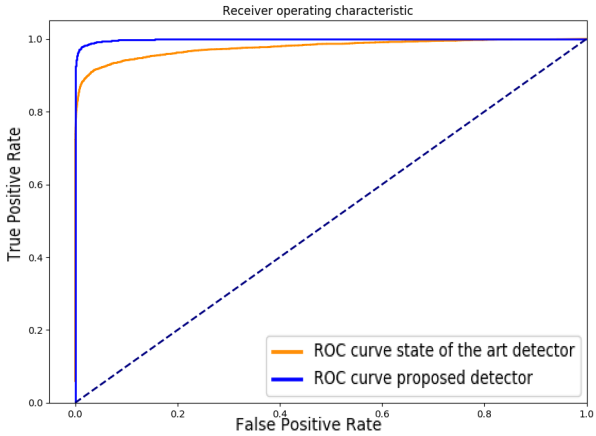

Figure 6 ROC curves for both state-of-the-art detector (orange) and proposed detector (blue)

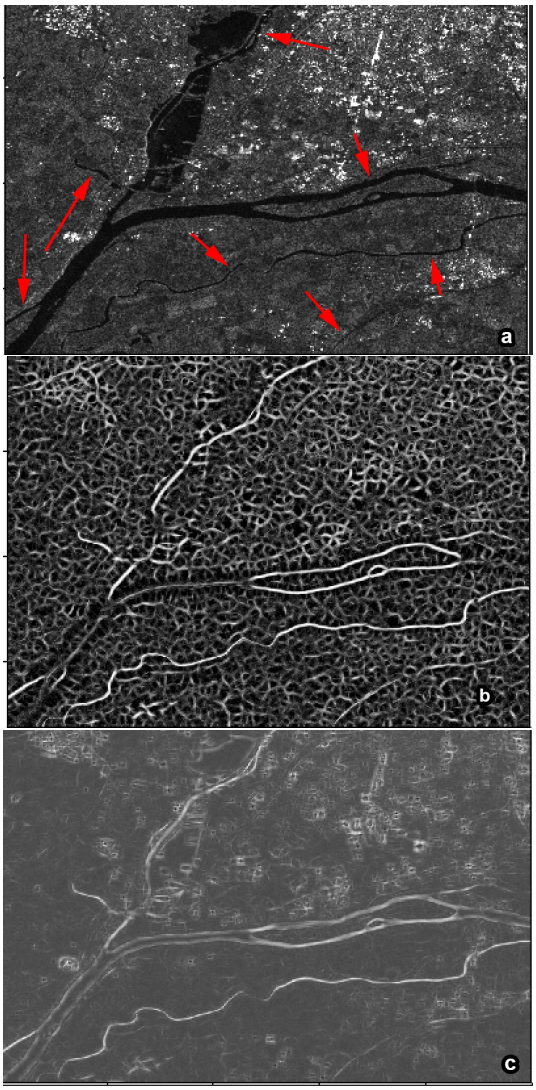

Figure 7 Comparison between the proposed detector (c) and the state-of-the-art detector (b) for one GRD image with linear structures highlighted by red arrows (a)